

Temporal spectrum of multiconjugate adaptive optics residuals and impact of tip-tilt anisoplanatism on astrometric observations

Giulia Carlà ^{*}, Cédric Plantet ^{*}, Lorenzo Busoni and Guido Agapito 

INAF, Osservatorio Astrofisico di Arcetri, Largo Enrico Fermi 5, I-50125 Firenze, Italy

Accepted 2022 August 10. Received 2022 August 4; in original form 2022 May 7

ABSTRACT

Multiconjugate adaptive optics (MCAO) will assist a new era of ground-based astronomical observations with the extremely large telescopes and the Very Large Telescope. High-precision relative astrometry is among the main science drivers of these systems and challenging requirements have been set for the astrometric measurements. A clear understanding of the astrometric error budget is needed and the impact of the MCAO correction has to be taken into account. In this context, we propose an analytical formulation to estimate the residual phase produced by an MCAO correction in any direction of the scientific field of view. The residual phase, computed in the temporal frequency domain, allows to consider the temporal filtering of the turbulent phase from the MCAO loop and to extract the temporal spectrum of the residuals, as well as to include other temporal effects such as the scientific integration time. The formulation is kept general and allows to consider specific frameworks by setting the telescope diameter, the turbulence profile, the guide stars constellation, the deformable mirrors configuration, the modes sensed and corrected, and the tomographic reconstruction algorithm. The formalism is presented for both a closed loop and a pseudo-open loop control. We use our results to investigate the effect of tip-tilt residuals on MCAO-assisted astrometric observations. We derive an expression for the differential tilt jitter power spectrum that also includes the dependence on the scientific exposure time. Finally, we investigate the contribution of the differential tilt jitter error on the future astrometric observations with MAVIS and MAORY.

Key words: instrumentation: adaptive optics – methods: analytical – astrometry.

1 INTRODUCTION

The next generation of ground-based telescopes equipped with adaptive optics (AO) will provide unprecedented resolutions to astronomical observations in the visible and near-infrared wavelengths. This is the case of the extremely large telescopes, the new class of 25–40 m telescopes observing in the near-infrared (Sanders 2013; Bigelow et al. 2020; Tamai et al. 2020), as well as the 8-m Very Large Telescope (VLT) observing in the visible (Arsenault et al. 2017). Most of the mentioned telescopes foresee the use of multiconjugate adaptive optics (MCAO; Beckers 1988; Rigaut & Neichel 2018) modules to compensate for the wavefront distortions induced by atmospheric turbulence: MAORY (Ciliegi et al. 2020) for the Extremely Large Telescope (ELT), NFIRAOS (Crane et al. 2018) for the Thirty Meter Telescope, and MAVIS (Rigaut et al. 2020) for the VLT. This flavour of AO aims to overcome the anisoplanatism problem, that represents a major limitation for single-conjugated adaptive optics (SCAO; Fried 1982; Chassat, Rousset & Primot 1989), through the use of both multiple guide stars (GSs) and deformable mirrors (DMs). The tomographic reconstruction of the turbulent volume from the GSs and the compensation for different layers of the atmosphere by the DMs help increase the isoplanatic patch, allowing the MCAO correction to provide uniform diffraction-limited images over wide fields of view. The high angular resolution, the uniformity of the correction over wide areas, the large number of

reference sources with high image quality provided, and the control of the field distortions through the DMs conjugated in altitude are characteristics that make MCAO a good candidate for astrometric observations. High-precision relative astrometry is, indeed, one of the main science drivers of the instruments equipped by the mentioned MCAO modules. The limiting astrometric precision is given by the centroiding error (Lindgren 1978) and leads to the challenging requirements that have been set for these systems: 50 μ s of astrometric precision for MAORY (goal of 10 μ s; Rodeghiero et al. 2019), 150 μ s for MAVIS (goal of 50 μ s; Monty et al. 2021), and 50 μ s for NFIRAOS (goal of 10 μ s; Schöck et al. 2014). It is then crucial to investigate all possible sources of error to keep the astrometric error budget within this fundamental limitation. An exhaustive list of the main contributions to the astrometric error in the case of MCAO-assisted observations was provided in Trippe et al. (2010). Among the sources of error mentioned, we are interested in investigating tip-tilt atmospheric residuals. In general, tip-tilt residuals affect the astrometric precision by introducing fluctuations of the position of a source with respect to the nominal position on the detector. On the one hand, the amount of fluctuations integrated during the individual exposure can determine an increasing of the size and a change in shape of the point spread function (PSF), with typical PSF elongation effect; on the other hand, if the fluctuations are not totally integrated within the exposure time of the image, a jitter of the source position can also be observed between successive frames. Relative astrometry, intended as the measurement of the distance between two distinct sources, can be affected by both effects: the former contributes to the centroiding error in measuring the position

^{*} E-mail: giulia.carla@inaf.it (GC); cedric.plantet@inaf.it (CP)

of each object, while the latter leads to the *differential tilt jitter* error, that is, the uncertainty in the distance measurement due to the relative residual jitter (Cameron, Britton & Kulkarni 2009; Fritz et al. 2010). The knowledge of the spatial and temporal dependence of tip-tilt residuals is needed to characterize the behaviour of the related astrometric error. For SCAO systems, tip-tilt anisoplanatism is well known and has been thoroughly modelled: measuring tip-tilt through an off-axis reference determines a residual tip-tilt on the target that linearly increases with the separation between the two sources, the linear dependence on the distance being valid for each pair of objects in the field (Sandler et al. 1994; Sasiela 1994; Hardy 1998). However, the characterization is more elaborate for the MCAO case, since the geometry with multiple GSs and multiple DMs needs to be taken into account and can lead to complex behaviours. As pointed out in Trippe et al. (2010), tip-tilt anisoplanatism is not well understood for this flavour of adaptive optics and, to our knowledge, an analysis does not exist yet. In this context, we propose an analytical formulation that allows the derivation of the temporal power spectral density (PSD) of the MCAO residual phase in any direction of the scientific field of view, by means of the spatiotemporal statistics of the turbulence-induced distortions and of the temporal transfer functions of an MCAO loop. The phase is intended as decomposed on a modal basis (e.g. Zernike modes, Noll 1976). Differently from existing approaches providing an estimation of MCAO residuals in the spatial frequency domain (e.g. Neichel, Fusco & Conan 2008), the presented method evaluates, for each mode, the MCAO residual phase in the temporal frequency domain and allows to include temporal effects such as the scientific integration time. The formulas are general and allow to analyse specific frameworks depending on the telescope aperture, the turbulence profile, the natural guide star (NGS) or laser guide star (LGS) asterism, the number and conjugation heights of the DMs, the sensed and corrected modes of distortion. The control loop and the tomographic reconstruction algorithm can also be chosen: in particular, we provide expressions in the case of either a closed-loop or a pseudo-open loop control. We then specialize our results to NGS-based systems and we analyse the behaviour of MCAO tip-tilt anisoplanatism. We model the effect on tip-tilt residuals of the scientific integration time as well. Moreover, we provide an analytical expression to derive the temporal PSD of differential tilt jitter. Finally, we show an application where we make use of the presented formulas to quantify the contribution of differential tilt jitter to the future MCAO-assisted astrometric observations, choosing MAORY and MAVIS as case studies.

In Section 2, we present the analytical approach and we derive the expression for the temporal PSD of the residual wavefront in the case of an MCAO correction; in Section 3, we use the formulas to analyse the spatial and temporal behaviour of tip-tilt residuals, as well as to provide the expression for the differential tilt jitter error; and in Section 4, we apply our results on differential tilt jitter to the MAORY and MAVIS cases.

2 TEMPORAL POWER SPECTRAL DENSITY OF MCAO WAVEFRONT RESIDUALS

The aim of this section is to derive an analytical expression of the residual phase produced by an MCAO correction in a generic direction of the field of view as a function of the temporal frequencies. From this quantity, the temporal PSD of the residual phase can be derived as

$$S_{\text{res}}^{\alpha}(\nu) = \langle \phi_{\text{res}}^{\alpha}(\nu) \phi_{\text{res}}^{\alpha \dagger}(\nu) \rangle, \quad (1)$$

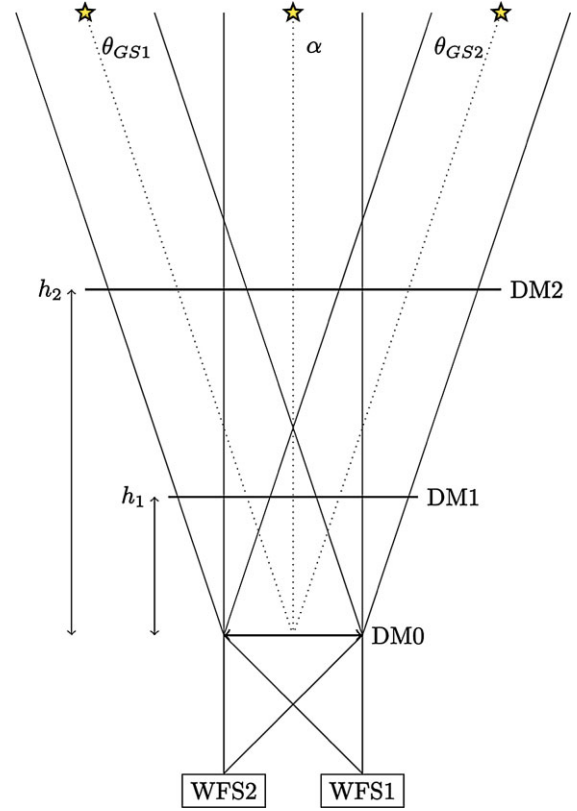


Figure 1. Scheme of the system geometry. In the example, there are two DMs conjugated at h_1 (DM1) and h_2 (DM2) and one at the ground layer (DM0), two GSs at coordinates θ_{GS1} and θ_{GS2} , and the scientific target at α . The wavefront distortion is measured by WFS1 and WFS2 looking at, respectively, GS1 and GS2.

where α identifies the position in the field of view, ν is the temporal frequency, $\langle \cdot \rangle$ is the ensemble average, \dagger denotes the conjugate-transpose, and ϕ represents the \mathcal{L} - or \mathcal{Z} -transform of the phase, depending on whether a continuous or discrete-time domain is considered. From the integration of $S_{\text{res}}^{\alpha}(\nu)$, the variance of the residual phase can be computed as well:

$$(\sigma_{\text{res}}^{\alpha})^2 = \int d\nu S_{\text{res}}^{\alpha}(\nu). \quad (2)$$

Among the sources of error contributing to the error budget of an MCAO correction, the presented method allows to take into account tomographic, noise, and temporal errors.

We consider the configuration in Fig. 1: the target and the GSs are, respectively, at positions α and $\theta_{GS} = [\theta_1, \theta_2, \dots, \theta_{N_{GS}}]$ with respect to the telescope's axis. The light from the sources passes through N_I layers of atmospheric turbulence before arriving at the pupil of the telescope. The turbulent layers are assumed to follow Taylor's frozen flow hypothesis. The turbulence-induced distortions are considered as decomposed on to wavefront modes and are measured by N_{GS} wavefront sensors (WFSs), each sensing n modes, and corrected by N_{DM} DMs optically conjugated at altitudes $h_{j=1}^{N_{DM}}$ and compensating a total of $m_{DM} = \sum_{k=1}^{N_{DM}} m_k$ modes. In the following, we will denote the turbulent and residual phase in the direction of the target as $\phi_{\text{turb}}^{\alpha}$ and $\phi_{\text{res}}^{\alpha}$, respectively, the turbulent and residual phase in the direction of the GSs as $\phi_{\text{turb}}^{\theta_{GS}}$ and $\phi_{\text{res}}^{\theta_{GS}}$, respectively, and the phase applied on the DMs as ϕ_{DM} . It follows that $\phi_{\text{turb}}^{\alpha}$ and $\phi_{\text{res}}^{\alpha}$ are vectors

of n elements, $\phi_{turb}^{\theta_{GS}}$ and $\phi_{res}^{\theta_{GS}}$ are vectors of $(n \cdot N_{GS})$ elements, and ϕ_{DM} is a vector of m_{DM} elements.

We start writing the residual phase along α as the difference between the turbulent phase and the correction phase, both evaluated in the direction of interest:

$$\begin{aligned}\phi_{res}^{\alpha}(v) &= \phi_{turb}^{\alpha}(v) - \phi_{corr}^{\alpha}(v) \\ &= \phi_{turb}^{\alpha}(v) - P_{DM}^{\alpha} \phi_{DM}(v),\end{aligned}\quad (3)$$

where ϕ_{corr}^{α} is the correction phase in the direction α , obtained through the matrix P_{DM}^{α} of size $n \times m_{DM}$ that projects the modes on the DMs as seen in the direction α on to the pupil. In the SCAO case, P_{DM}^{α} is the identity for any direction α as the correction is common to all directions of the field of view ($\phi_{corr}^{\alpha} = \phi_{corr}$). We define $\phi_{DM}(v)$ as

$$\phi_{DM}(v) = H_{ol}(v)W(\phi_{res}^{\theta_{GS}}(v) + \phi_n(v)), \quad (4)$$

where H_{ol} is the open-loop transfer function of the AO feedback loop, W is the reconstruction matrix, with dimension $m_{DM} \times (n \cdot N_{GS})$, relating the modes measured by the WFSs and the ones to be applied by the DMs, and $\phi_n(v)$ is the WFSs measurement noise on the modes. We assumed ideal WFSs, meaning that they perform a direct measurement of the phase. In the case of a pure integrator, the expression of H_{ol} is (Madec 1999; Correia et al. 2017):

$$\begin{aligned}H_{ol}(s) &= H_{wfs}(s)H_c(s) \\ &= \frac{(1 - e^{-sT})}{sT} \frac{g}{sT} e^{-sT_d},\end{aligned}\quad (5)$$

where we limited the contributors to the wavefront sensor and the control and where $s = i2\pi\nu$ is the Laplace variable, g is the gain, $T = 1/\nu_{loop}$ with ν_{loop} the loop frequency, T_d is the delay time of the control and where we defined $H_{wfs}(s) = (1 - e^{-sT})/sT$ and $H_c(s) = g/sT e^{-sT_d}$.

By replacing equation (4) in equation (3) as referred to the GSs directions ($\alpha = \theta_{GS}$), we get an expression of the residual phase on the GSs:

$$\begin{aligned}\phi_{res}^{\theta_{GS}}(v) &= (Id + P_{DM}^{\theta_{GS}} H_{ol}(v)W)^{-1} \phi_{turb}^{\theta_{GS}}(v) \\ &\quad - (Id + P_{DM}^{\theta_{GS}} H_{ol}(v)W)^{-1} P_{DM}^{\theta_{GS}} H_{ol}(v)W \phi_n(v) \\ &= H_r(v) \phi_{turb}^{\theta_{GS}}(v) - H_n(v) \phi_n(v),\end{aligned}\quad (6)$$

where $P_{DM}^{\theta_{GS}}$ is the DMs-WFSs projection matrix, with dimension $(n \cdot N_{GS}) \times m_{DM}$ and Id is an $(n \cdot N_{GS}) \times (n \cdot N_{GS})$ identity matrix. We defined

$$H_r(v) = (Id + P_{DM}^{\theta_{GS}} H_{ol}(v)W)^{-1} \quad (7)$$

as the rejection transfer function (RTF), and

$$H_n(v) = (Id + P_{DM}^{\theta_{GS}} H_{ol}(v)W)^{-1} P_{DM}^{\theta_{GS}} H_{ol}(v)W \quad (8)$$

as the noise transfer function (NTF) of the MCAO loop. It is worth noting that these expressions also include a dependence on the spatial reconstruction. If taking the SCAO limit, $P_{DM}^{\theta_{GS}}$ and W become equal to one and the classical definitions of RTF and NTF are retrieved (Agapito, Arcidiacono & Esposito 2017).

We then replace equation (6) in equation (4):

$$\begin{aligned}\phi_{DM}(v) &= H_{ol}(v)W(H_r(v) \phi_{turb}^{\theta_{GS}}(v) - H_n(v) \phi_n(v) + \phi_n(v)) \\ &= H_{ol}(v)W H_r(v) (\phi_{turb}^{\theta_{GS}}(v) + \phi_n(v)) \\ &= H_{n,tomo}(v) (\phi_{turb}^{\theta_{GS}}(v) + \phi_n(v)),\end{aligned}\quad (9)$$

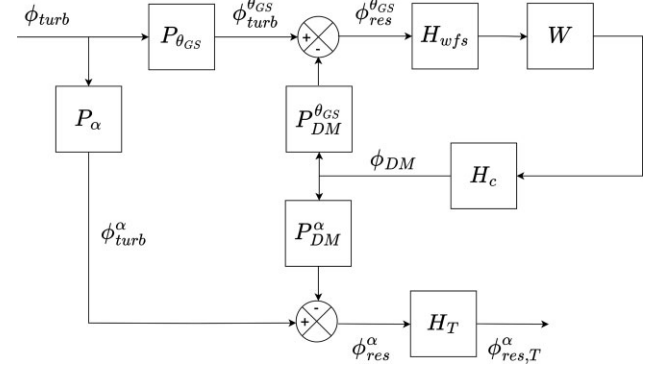


Figure 2. Diagram of the control loop. The phase on the DMs is controlled in closed loop from the measurements on the GSs and its projection along α determines the residual phase on the target in α . The $P_{\theta_{GS}}$ and P_{α} blocks have been introduced as projections of the turbulent phase on to θ_{GS} ($\phi_{turb}^{\theta_{GS}} = P_{\theta_{GS}} \phi_{turb}$) and α ($\phi_{turb}^{\alpha} = P_{\alpha} \phi_{turb}$), respectively. The H_T block represents the temporal filtering by the scientific instrument, as it will be shown in Section 3.2.

where we used the relation $H_r(v) + H_n(v) = Id$, as derived from the sum of equations (7) and (8), and where we defined the matrix $H_{n,tomo}(v) = H_{ol}(v)WH_r(v)$ as a tomographic NTF.

By substituting equation (9) in equation (3), we derive a final expression for the residual phase along α :

$$\begin{aligned}\phi_{res}^{\alpha}(v) &= \phi_{turb}^{\alpha}(v) - P_{DM}^{\alpha} [H_{n,tomo}(v) (\phi_{turb}^{\theta_{GS}}(v) + \phi_n(v))] \\ &= \phi_{turb}^{\alpha}(v) - H_{n,tomo}^{\alpha}(v) (\phi_{turb}^{\theta_{GS}}(v) + \phi_n(v)),\end{aligned}\quad (10)$$

where $H_{n,tomo}^{\alpha}(v) = P_{DM}^{\alpha} H_{n,tomo}(v)$ is the tomographic NTF projected along α . The diagram of the control loop described is shown in Fig. 2.

From equations (1) and (10), we can also compute the temporal power spectrum of the residual phase along α :

$$\begin{aligned}S_{res}^{\alpha}(v) &= S_{turb}^{\alpha}(v) + H_{n,tomo}^{\alpha}(v) (S_{turb}^{\theta_{GS}}(v) + S_n(v)) H_{n,tomo}^{\alpha \dagger}(v) \\ &\quad - 2Re(H_{n,tomo}^{\alpha}(v) S_{turb}^{\theta_{GS},\alpha}(v)),\end{aligned}\quad (11)$$

where S_{turb}^{α} is the temporal PSD of the turbulence, $S_{turb}^{\theta_{GS}}$ is the temporal PSD of the turbulence on the GSs directions, S_n is the temporal PSD of the noise and $S_{turb}^{\theta_{GS},\alpha}$ is the cross PSD (CPSD) (Plantet et al. 2022) of the turbulence between the GSs and the target. We assumed turbulence and noise to be uncorrelated. The derived expression can provide a fast evaluation of the MCAO residuals in the field of view, given a statistics of turbulence and noise and the temporal filtering operated by the AO loop. It is worth noting that the SCAO limit of equation (11) gives the same expression as provided in equation (54) of Plantet et al. (2022).

Another version of equations (10) and (11) can be obtained if not only one target, but a set of targets equaling the number of GSs is considered ($\alpha = [\alpha_1, \alpha_2, \dots, \alpha_{N_{GS}}]$). In this case, we can modify equation (10) as

$$\begin{aligned}\phi_{res}^{\alpha}(v) &= \phi_{turb}^{\alpha}(v) - H_{n,tomo}^{\alpha}(v) (\phi_{turb}^{\theta_{GS}}(v) + \phi_n(v)) \\ &= Id \phi_{turb}^{\alpha}(v) - H_{n,tomo}^{\alpha}(v) (\phi_{turb}^{\theta_{GS}}(v) + \phi_n(v)) \\ &= H_{r,tomo}^{\alpha}(v) \phi_{turb}^{\alpha}(v) \\ &\quad - H_{n,tomo}^{\alpha}(v) (\phi_{turb}^{\theta_{GS}}(v) - \phi_{turb}^{\alpha}(v) + \phi_n(v)),\end{aligned}\quad (12)$$

where $H_{r,tomo}^{\alpha}$ is the tomographic RTF projected along α , defined so that the relation $H_{r,tomo}^{\alpha}(v) + H_{n,tomo}^{\alpha}(v) = Id$ holds. This expression allows to differentiate the various contributions due to the rejection of

turbulence (first term), to generalized anisoplanatism that is filtered as a noise by the AO loop (second plus third term) and to noise (last term). This is also shown by deriving the related temporal power spectrum:

$$\begin{aligned} S_{res}^{\alpha}(v) = & H_{r,tomo}^{\alpha}(v) S_{turb}^{\alpha}(v) H_{r,tomo}^{\alpha \dagger}(v) \\ & + H_{n,tomo}^{\alpha}(v) S_n(v) H_{n,tomo}^{\alpha \dagger}(v) \\ & + H_{n,tomo}^{\alpha}(v) (S_{turb}^{\theta GS}(v) - S_{turb}^{\alpha}(v)) H_{n,tomo}^{\alpha \dagger}(v) \\ & + 2Re \left[H_{n,tomo}^{\alpha}(v) (S_{turb}^{\alpha} - S_{turb}^{\theta GS}) \right], \end{aligned} \quad (13)$$

where the first and second term leads, respectively, to the temporal and noise error, while the remaining terms quantify the tomographic error as well as its temporal filtering by the MCAO loop.

2.1 Pseudo-open loop control + MMSE reconstruction

In the previous calculations, we considered a closed-loop control, that is, the reconstruction is performed on the residual measurements as shown in equation (4). The reconstruction matrix W is then intended as the pseudo-inverse of the projection matrix $P_{DM}^{\theta GS}$, as derived in the least square estimator (LSE) approach (Madec 1999). However, it has been demonstrated not to be the optimal approach to deal with the problem of badly and unseen modes (Fusco et al. 2001a, b; Le Roux et al. 2004; Neichel et al. 2008) characterizing MCAO correction and that the minimum mean square error (MMSE) approach can lead to better performance, even if compared to the truncated LSE (TLSE; Quiros-Pacheco et al. 2004). As the MMSE reconstructor operates on the pseudo-open loop measurements of the turbulent phase, it has to be included in a pseudo-open loop control (POLC) (Ellerbroek & Vogel 2003). In this context, we provide the expressions to derive the performance of MCAO systems also in the case of POLC and MMSE.

We modify equation (4) in order to consider a reconstruction acting on the pseudo-open loop measurements (Basden et al. 2019):

$$\phi_{DM}(v) = H_{ol}(v) (W_{MMSE} \phi_{OL}^{\theta GS}(v) - \phi_{DM}(v)), \quad (14)$$

where W_{MMSE} is the MMSE reconstructor and $\phi_{OL}^{\theta GS}$ are the open-loop measurements that we write as

$$\phi_{OL}^{\theta GS}(v) = \phi_{res}^{\theta GS}(v) + \phi_n(v) + P_{DM}^{\theta GS} \phi_{DM}(v). \quad (15)$$

We replace this expression in equation (14):

$$\begin{aligned} \phi_{DM}(v) = & H_{ol}(v) \left[W_{MMSE} (\phi_{res}^{\theta GS}(v) + \phi_n(v) \right. \\ & \left. + P_{DM}^{\theta GS} \phi_{DM}(v)) - \phi_{DM}(v) \right] \\ = & H_{ol}(v) W_{MMSE} (\phi_{res}^{\theta GS}(v) + \phi_n(v)) \\ & + H_{ol}(v) (W_{MMSE} P_{DM}^{\theta GS} - Id) \phi_{DM}(v). \end{aligned} \quad (16)$$

We group the terms related to ϕ_{DM} :

$$\begin{aligned} & [Id - H_{ol}(v) (W_{MMSE} P_{DM}^{\theta GS} - Id)] \phi_{DM}(v) \\ = & H_{ol}(v) W_{MMSE} (\phi_{res}^{\theta GS}(v) + \phi_n(v)), \end{aligned} \quad (17)$$

and we obtain a final expression of the DMs phase:

$$\begin{aligned} \phi_{DM}(v) = & [Id - H_{ol}(v) (W_{MMSE} P_{DM}^{\theta GS} - Id)]^{-1} \\ & \times H_{ol}(v) W_{MMSE} (\phi_{res}^{\theta GS}(v) + \phi_n(v)) \\ = & [Id + H_{ol}(v) K]^{-1} H_{ol}(v) W_{MMSE} (\phi_{res}^{\theta GS}(v) + \phi_n(v)) \\ = & H_{polc}(v) W_{MMSE} (\phi_{res}^{\theta GS}(v) + \phi_n(v)), \end{aligned} \quad (18)$$

where we defined the matrices $K = Id - W_{MMSE} P_{DM}^{\theta GS}$ and $H_{polc} = [Id + H_{ol}(v) K]^{-1} H_{ol}(v)$.

It follows that the results in equations (10) and (11) can still be used to compute the residual phase and PSD on target, but considering $H_{ol} = H_{polc}$ and $W = W_{MMSE}$ when taking into account POLC + MMSE.

3 TIP-TILT ANISOPLANATISM IN MCAO-ASSISTED ASTROMETRIC OBSERVATIONS

In this section, we use the formulation introduced in Section 2 as a tool to investigate the behaviour of atmospheric tip-tilt residuals in MCAO-assisted observations and their impact on astrometric precision. Since, in the presented approach, the phase is intended as decomposed on to wavefront modes, we can derive the temporal PSD and the variance of tip-tilt residuals from equations (11) and (2), respectively, by applying both equations to tip and tilt modes.

Throughout the following analysis, we consider the contribution of all the modes to the turbulence-induced wavefront distortions and a reconstruction of tip-tilt at the ground and focus-astigmatism at the high layer, based on the tip-tilt measurements from three NGSs in equilateral asterism. Such NGS loop can be used for the control of the *null modes* (Flicker, Rigaut & Ellerbroek 2003) in MCAO systems using a split tomography approach (Gilles & Ellerbroek 2008). The compensation for focus-astigmatism at the pupil plane is not included in our configuration and this would provide an out of focus and astigmatic PSF; however, this is not a limitation for our analysis as we are interested in investigating the variations of tip-tilt in the field of view. As we do not consider the LGS-based correction of the higher orders, the results have to be intended as an upper limit to the atmospheric tip-tilt residuals. An extended study including the LGS loop will be the object of future works. We use an LSE reconstructor, as the control of modes up to the astigmatism with a symmetric asterism and without noise does not foresee divergences in the system's behaviour; thus, it does not require a threshold nor an MMSE reconstructor, as it would be expected in the real cases.

First, we analyse the dependence of on-axis tip-tilt residuals on the NGS asterism. Then, we introduce the contribution of the scientific integration time and, finally, we estimate relative tip-tilt residuals, that is the amount of differential tilt jitter error.

3.1 On-axis tip-tilt residuals

We consider the DM0 at 0 m and the DM1 at 17 km. We assume an equilateral asterism of NGSs centred at the origin of the field of view. We consider a 40-m telescope and the ELT median turbulence profile reported in Sarazin et al. (2013), with a seeing of 0.644 arcsec and an average wind speed of 9.2 m s⁻¹. As we are mainly interested in the analysis of spatial anisoplanatism, we neglect the noise assuming NGSs with infinite flux. We also minimize the temporal error considering a loop with a frequency frame rate of 1 kHz and where the control is a pure integrator with a delay given by the WFSs exposure time only.

In Fig. 3, we show the dependence on the asterism radius of tip-tilt residuals for a target on axis. The errors are computed from the integration of equation (11), applied to tip-tilt, over the temporal frequencies. The MCAO residuals are shown in comparison to the SCAO case, where the asterism radius becomes the angular separation of the NGS from the target; as expected from the larger isoplanatic patch provided by the MCAO correction, MCAO errors

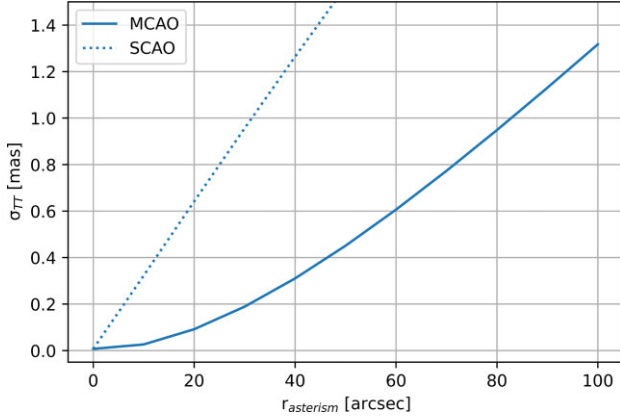


Figure 3. Tip-tilt residuals for a target at the origin of the field of view, as functions of the radius of the NGS asterism. The SCAO limit is also shown for comparison (dotted line); in this case, the values on the x -axis represent the angular separation between the target and the NGS.

are reduced with respect to the SCAO ones. Moreover, we note that, differently from the SCAO case, whose errors linearly depend on the off-axis separation, MCAO residuals show a quadratic dependence on the NGSs separation. We can explain the different behaviours as follows: the turbulence-induced distortions that are observed on the pupil plane can be described by a combination of polynomials with increasing degree:

$$\begin{aligned}\Delta x &= a_1 + a_2x + a_3y + a_4x^2 + a_5xy + a_6y^2 + \dots \\ \Delta y &= b_1 + b_2y + b_3x + b_4y^2 + b_5yx + b_6x^2 + \dots,\end{aligned}\quad (19)$$

where the zeroth-order coefficients (a_1, b_1) represent a global tip-tilt, that is a shift in x and y common to all directions of the field of view, the first order coefficients (a_2, a_3, b_2, b_3) represent the plate-scale distortions produced by the projection of focus and astigmatism in altitude on to the tip-tilt in pupil, and so on for the higher orders. The covariance matrix of the distortions is $\langle \Delta \mathbf{r} \Delta \mathbf{r}^T \rangle$, with $\Delta \mathbf{r} = (\Delta x, \Delta y)$. The SCAO, correcting with only a DM at the ground and using a single WFS, is able to compensate for the zeroth order of the distortions (i.e. overall pointing), leaving residual distortions that are then dominated by the first order (i.e. plate-scale variations). The MCAO, in our NGS-based configuration, removes a global tip-tilt with the DM0 and, in addition, is able to control the first-order distortions by compensating for focus and astigmatism with the DM1 conjugated in altitude. The residual distortions are, in this case, dominated by the second order. The sum of the diagonal terms of the residual distortions covariance matrix leads, for the SCAO case, to the following expression:

$$\begin{aligned}\sum_{i=1,2} \langle \Delta \mathbf{r} \Delta \mathbf{r}^T \rangle_{ii} &= (a_2x + a_3y + \dots)^2 + (b_2y + b_3x + \dots)^2 \\ &= u(x^2 + y^2) + \dots,\end{aligned}\quad (20)$$

and, for the MCAO case, to:

$$\begin{aligned}\sum_{i=1,2} \langle \Delta \mathbf{r} \Delta \mathbf{r}^T \rangle_{ii} &= (a_4x^2 + a_5xy + a_6y^2 + \dots)^2 \\ &\quad + (b_4y^2 + b_5yx + b_6x^2 + \dots)^2 \\ &= v(x^2 + y^2)^2 + \dots,\end{aligned}\quad (21)$$

where the simplification in the coefficient u for the former and v for the latter is obtained by replacing the coefficients of the polynomial series with the proper coefficients that relate tip-tilt on the pupil plane with the higher orders on a meta-pupil in altitude (see Appendix A).

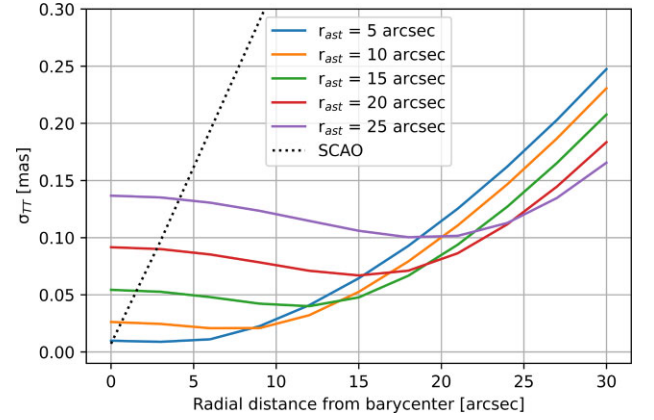


Figure 4. Tip-tilt residuals as functions of the target's radial distance with respect to the origin. The curves are shown for different values of the NGS asterism radius (r_{ast}) and the SCAO limit is also shown (dotted line).

If we consider (x, y) as the position of the target with respect to the NGS, we find a dependence of the variance on the second power of the separation for the SCAO case and on the fourth power for the MCAO case.

In Fig. 4, we show the spatial distribution of tip-tilt residuals in the field of view. The errors are computed for targets at different radial separations from the origin (that also represents the barycentre of the asterism), the final values being obtained from the average over several polar angles in order not to be affected by the geometry of the asterism. The errors show similar values for targets within the NGS asterism and increase outside of the asterism, where tip-tilt is indeed not controlled. The minimum of the curves is not exactly at a distance equal to the asterism radius value, depending on the fact that the targets at an angular separation equal to the asterism radius fall outside of the NGSs triangle (except the ones with the same exact polar angles as the NGSs ones), where tip-tilt is worse controlled.

3.2 Scaling of tip-tilt residuals with the scientific integration time

The previous results, obtained from a pure integration of equation (11), represent the case where the fluctuations in position due to tip-tilt residuals are fully integrated within the exposure and thus impact entirely on the shape and size of the PSF, leading to the PSF elongation. This effect contributes to the astrometric error due to photon noise (Lindgren 1978):

$$\sigma \sim \frac{FWHM}{SNR}, \quad (22)$$

where $FWHM$ is the full width at half maximum of the PSF and SNR is the signal-to-noise ratio. Regardless of the residual value contributing to the FWHM, this source of error can be ideally reduced to zero if we assume a source with infinite SNR. In this case, tip-tilt residuals would not affect the astrometric precision. On the other hand, if tip-tilt residuals are not fully integrated within the exposure, fluctuations in position due to the residual jitter are observed between successive frames, these affecting astrometric precision despite the source flux. Thanks to the knowledge of the temporal PSD of the residuals, we can analytically describe the residual jitter between successive frames by still following an approach that makes use of temporal transfer functions, as in Section 2.

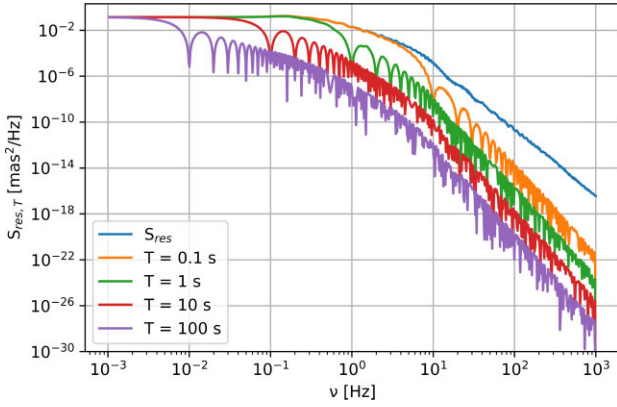


Figure 5. Temporal power spectrum of the residual jitter between successive frames, for scientific exposures of 0.1 s (orange), 1 s (green), 10 s (red), and 100 s (purple). The configuration is the same as Fig. 3, with a target on axis and an asterism radius of 40 arcsec. The unaveraged tip-tilt residual PSD is also shown for comparison (blue).

We write the expression of the phase residuals that are left after a scientific integration of length T as

$$\phi_{res,T}^\alpha(\nu) = H_T(\nu)\phi_{res}^\alpha(\nu), \quad (23)$$

where ϕ_{res}^α is given by equation (10) and H_T is the temporal transfer function of the scientific camera, that is the Laplace or Z-transform of the time-average operation. In the Laplace case, the expression is given by

$$\begin{aligned} H_T(\nu) &= \frac{1}{T} \tilde{\Pi}_T(\nu) \\ &= \text{sinc}(\pi\nu T) e^{-i\pi\nu T}, \end{aligned} \quad (24)$$

where $\tilde{\Pi}_T$ denotes the transform of the rectangular function Π_T . From equations (1) and (23), we can get the expression of the residual PSD for scientific frames of length T :

$$S_{res,T}^\alpha(\nu) = |H_T(\nu)|^2 S_{res}^\alpha(\nu), \quad (25)$$

where S_{res}^α is given by equation (11).

The results of this expression, as applied to tip and tilt, are shown in Fig. 5, where on-axis tip-tilt residual PSDs are plotted for different integration times. The impact of the scientific exposure depends on the relation between the cut-off frequency of the camera transfer function and the one of the residual PSD. The camera transfer function acts as a low-pass filter with a cut-off frequency $\nu_{H_{sci}} = 1/T$. If $\nu_{H_{sci}}$ is either larger or about the same as the tip-tilt residual PSD cut-off frequency ($\nu_{S_{res}} \simeq 0.6 \nu/D$, with ν the wind velocity and D the telescope diameter; Conan, Rousset & Madec 1995), the scientific integration is not long enough to average the residuals and the position jitter observed between different exposures is emphasized. Indeed, in this case, the camera is either unable to filter any frequency of the PSD, or it filters only the frequencies that are larger than $\nu_{S_{res}}$, where the energy falls rapidly to zero. As the integration time increases, $\nu_{H_{sci}}$ becomes smaller than $\nu_{S_{res}}$ and the camera transfer function passes the frequencies where the PSD is flat, leaving then a residual variance that is proportional to $1/T$. Thus, the root mean square (rms) is proportional to $T^{-1/2}$. This behaviour is shown in Fig. 6: for integration times smaller than the inverse of $\nu_{S_{res}}$, tip-tilt residuals do not depend on T and the curve is flat, while it follows a $T^{-1/2}$ law for larger times. The $T^{-1/2}$ power law is in agreement with the assumptions and the results that are present

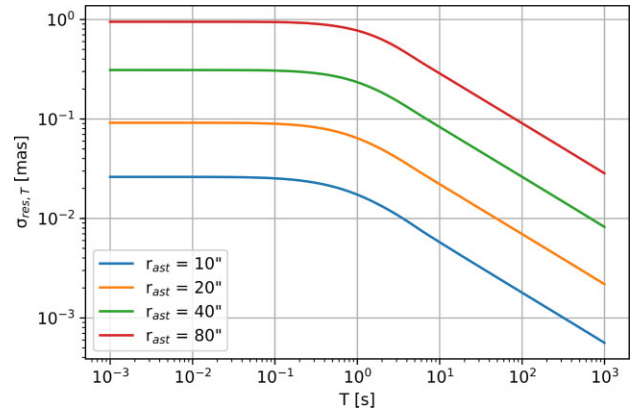


Figure 6. Tip-tilt residual error on axis as a function of the scientific integration time. The configuration is the same as Fig. 5, with the asterism radius varying from 10 to 80 arcsec.

in the literature (Ellerbroek 2007; Cameron et al. 2009; Ammons, Bendek & Guyon 2011).

3.3 Differential tilt jitter

The results in Section 3.2 give information about the repeatability of the position measurement of a single source. However, the science cases of future instruments show a major interest in relative astrometry, that is, in measuring the distance between sources. To be able to estimate the precision in the distance measurements, we extend the analysis to differential tilt jitter. This effect is well known for SCAO systems but, to our knowledge, is less well understood and no expression is present in the literature to compute this error for MCAO systems. In this context, we present an analytical expression for this flavour of adaptive optics as well, by using the results in Section 2.

We consider two sources in directions α and β and we describe the differential jitter phase through the difference between the residual phases in the two directions:

$$\phi_{DTJ}^{\alpha,\beta}(\nu) = \phi_{res}^\alpha(\nu) - \phi_{res}^\beta(\nu). \quad (26)$$

The temporal PSD is then

$$\begin{aligned} S_{DTJ}^{\alpha,\beta}(\nu) &= \langle \phi_{DTJ}^{\alpha,\beta}(\nu) \phi_{DTJ}^{\alpha,\beta\dagger}(\nu) \rangle \\ &= \langle (\phi_{res}^\alpha(\nu) - \phi_{res}^\beta(\nu)) (\phi_{res}^\alpha(\nu) - \phi_{res}^\beta(\nu))^\dagger \rangle. \end{aligned} \quad (27)$$

For SCAO systems, the difference between residual phases simplifies into the difference between turbulent phases because, as already pointed out in Section 2, the correction phase is common to all directions. The reasoning leads to the following expression of differential tilt jitter PSD for the SCAO case:

$$S_{DTJ}^{\alpha,\beta}(\nu) = 2(S_{turb}(\nu) - S_{turb}^{\alpha,\beta}(\nu)), \quad (28)$$

where $S_{turb}^{\alpha,\beta}$ is the CPSD of turbulence between the two directions and where we considered $S_{turb} = S_{turb}^\alpha = S_{turb}^\beta$, having assumed a homogeneous and isotropic turbulence. The expression (integrated over the temporal frequencies) is in agreement with the results that are present in the literature (Sandler et al. 1994; Cl  net et al. 2015).

For MCAO systems, we can replace ϕ_{res}^α and ϕ_{res}^β with the expression in equation (10) applied to α and β , respectively. We

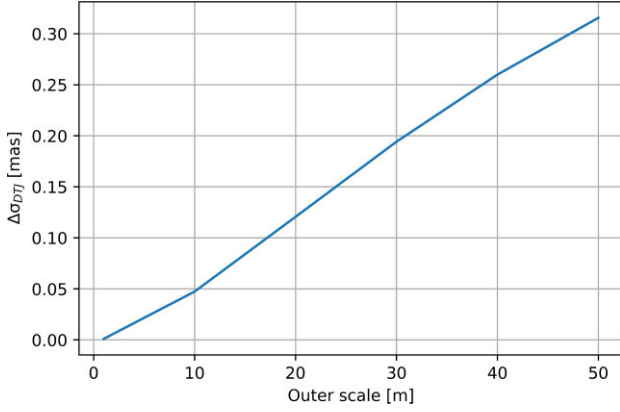


Figure 7. Difference between SCAO and MCAO differential tilt jitter error ($\Delta\sigma_{DTJ} = \sqrt{\sigma_{DTJ,SCAO}^2 - \sigma_{DTJ,MCAO}^2}$) as a function of the outer scale. The telescope, DMs, NGSs, turbulence configurations are the same as in Fig. 3. The targets' angular separation is 5 arcsec and the asterism radius is 40 arcsec.

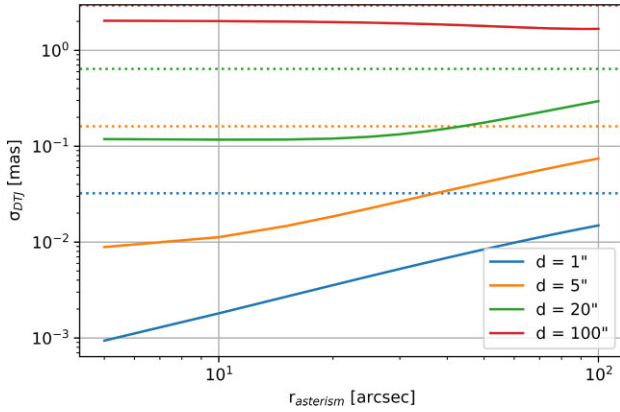


Figure 8. MCAO differential tilt jitter error as a function of the NGS asterism radius. The colours show different values of the distance between the astrometric targets. For each curve, the SCAO case is shown as comparison (dotted lines).

obtain

$$S_{DTJ}^{\alpha,\beta}(v) = 2(S_{turb}(v) - S_{turb}^{\alpha,\beta}(v)) + \Delta H_{n,tomo}^{\alpha,\beta}(v)(S_{turb}^{\theta_{GS}}(v) + S_{noise}(v))\Delta H_{n,tomo}^{\alpha,\beta}(v)^{\dagger} - 2Re[\Delta H_{n,tomo}^{\alpha,\beta}(v)(S_{turb}^{\theta_{GS},\alpha}(v) - S_{turb}^{\theta_{GS},\beta}(v))], \quad (29)$$

where we defined $\Delta H_{n,tomo}^{\alpha,\beta}(v) = H_{n,tomo}^{\alpha}(v) - H_{n,tomo}^{\beta}(v)$. It is worth noting that, if taking the SCAO limit of this expression, we get $H_{n,tomo}^{\alpha} = H_{n,tomo}^{\beta}$ and we retrieve the results in equation (28). Equation (29) shows that differential tilt jitter error in MCAO systems is given by the SCAO case error (first two terms) and additional terms depending on the correction (asterism/targets geometry, temporal filtering of the AO loop, noise) and on spatiotemporal cross-correlations of the turbulence. These additional terms might reduce the error with respect to the SCAO case, as shown in Figs 7 and 8. In the former, the rms of the difference between the variances obtained from equations (28) and (29) as a function of the outer scale is plotted. As expected, the discrepancy between the SCAO and MCAO values increases with the outer scale, as a larger outer scale leads to larger cross-correlations that help reduce the differential tilt jitter error in the MCAO correction. In the latter, the MCAO differential tilt jitter

Table 1. Telescope diameter, DMs conjugation height, set of asterism radii, and scientific field of view radius used to derive the differential tilt jitter error for MAVIS- and MAORY-assisted observations. The outer scale used for both cases is 25 m.

	MAVIS	MAORY
D (m)	8	39
h_{DM0} (m)	0	600
h_{DM1} (m)	13 500	17 000
$r_{asterism}$ (arcsec)	10, 30, 50, 60	30, 55, 70, 80
r_{FoV} (arcsec)	15	30

error as a function of the NGS asterism radius is shown. The smaller cross-correlations given by larger asterisms determine an increasing of the differential tilt jitter error with the asterism radius. This is evident when the distance is small and both targets are included within the asterism ($d = 1$ arcsec, 5 arcsec); for larger distances, the errors are about constant up to an asterism radius comparable to the targets' separation and then show the increasing behaviour.

As in Section 3.2, we can also take into account the contribution of the scientific exposure on the differential tilt jitter error, through the temporal filtering of the camera integrating over T :

$$\phi_{DTJ,T}^{\alpha,\beta}(v) = H_T(v)(\phi_{res}^{\alpha}(v) - \phi_{res}^{\beta}(v)). \quad (30)$$

The PSD of time-averaged differential tilt jitter is then

$$S_{DTJ,T}^{\alpha,\beta}(v) = |H_T(v)|^2 S_{DTJ}^{\alpha,\beta}(v), \quad (31)$$

where $S_{DTJ}^{\alpha,\beta}$ is given by equation (28) for SCAO and by equation (29) for MCAO.

4 APPLICATION: DIFFERENTIAL TILT JITTER ERROR FOR MAVIS AND MAORY

In this section, we use equation (29) to investigate the contribution of differential tilt jitter error on the future astrometric observations; as case studies, we consider MAVIS at the VLT and MAORY at the ELT.

In Table 1, we summarize the main parameters that we used to describe the two systems. The maximum value of the asterism radius represents the technical field of view (120 arcsec for MAVIS and 160 arcsec for MAORY). As in Section 3, we assume equilateral asterisms of NGS with infinite flux to neglect the contribution of noise. The measurements from the three NGSs allow to reconstruct tip and tilt, that are corrected on the DM0, and focus-astigmatism, applied on the DM1. We consider a closed loop, where the control is a pure integrator working at 1 kHz and where we minimize the latency by considering a delay due to the WFSs integration time only. For the computation of the PSDs and CPSDs of turbulence, we used the same turbulence profile as in Section 3, with a zenith angle of 30° .

In Fig. 9, we show the differential tilt jitter error for MAVIS and MAORY, obtained for typical scientific exposures of $T = 30$ s. The error is computed considering the first source at the origin of the field of view and varying the distance of the second source up to the edge of the scientific field of view.

In order not to be affected by the geometry of the asterism of NGSs, for each separation we made an azimuthal average of the errors obtained at different polar coordinates. The plots show that differential tilt jitter can introduce errors on relative astrometry up to

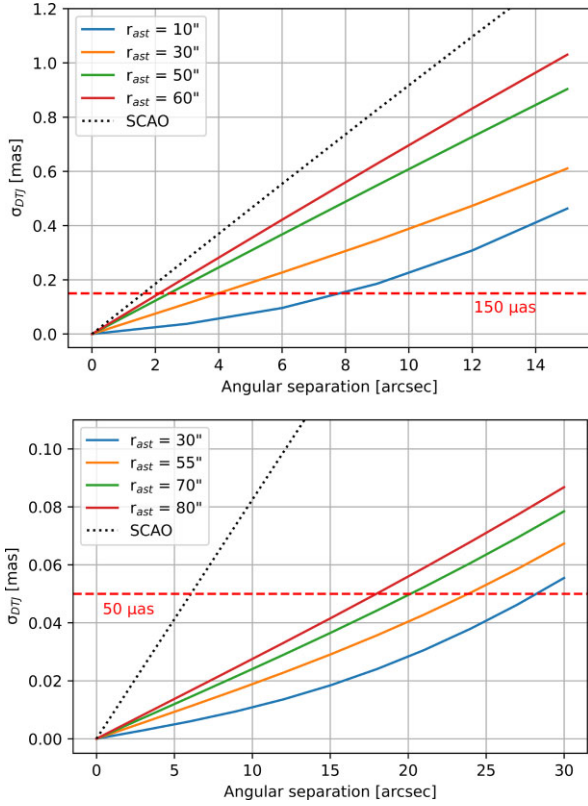


Figure 9. Differential tilt jitter error as a function of the angular separation for MAVIS- (top) and MAORY- (bottom) assisted observations of length $T = 30$ s. The SCAO case (dotted black line) is shown for comparison, as well as the astrometric precision requirement (dashed red line) of the two systems.

~ 0.4 – 1 mas for MAVIS and ~ 60 – 90 μas for MAORY at the edge of the field of view. As shown in Section 3.2, this source of error can be reduced with the integration time; if the measurements, for instance, can be averaged over ~ 30 min of exposures, the relative astrometric error due to differential tilt jitter is reduced by a factor of ~ 8 and becomes smaller than the requirement value over the whole field of view for both cases.

Current specifications suggest a major interest in high-precision relative astrometry for separations up to 1 arcsec (Rigaut et al. 2020). For a better visualization of this scale, in Fig. 10 we show the differential tilt jitter error as a function of the asterism radius for a fixed distance of 1 arcsec. The plots show that differential tilt jitter error should not represent a relevant contribution to the MAORY astrometric error budget for these separations, even considering the goal of 10 μas . For MAVIS, the error shows to be within the requirement of 150 μas , but not compliant with the goal of 50 μas for asterisms with radius larger than 40 arcsec and for the typical exposure time of 30 s. In this case, the possibility to average over longer integration times is required.

It is worth pointing out that these results show the contribution of atmospheric tip-tilt residuals in terms of differential tilt jitter only. The contribution of tip-tilt residuals on the astrometric error in terms of the centroiding error is not considered (that is equivalent to assume targets with infinite SNR). Moreover, the contribution of temporal errors of the AO loop is minimized and noise terms are neglected. On the other hand, it should be considered that the differential tilt jitter error could be calibrated out through dedicated coordinate transforms, if reference sources are available in the field

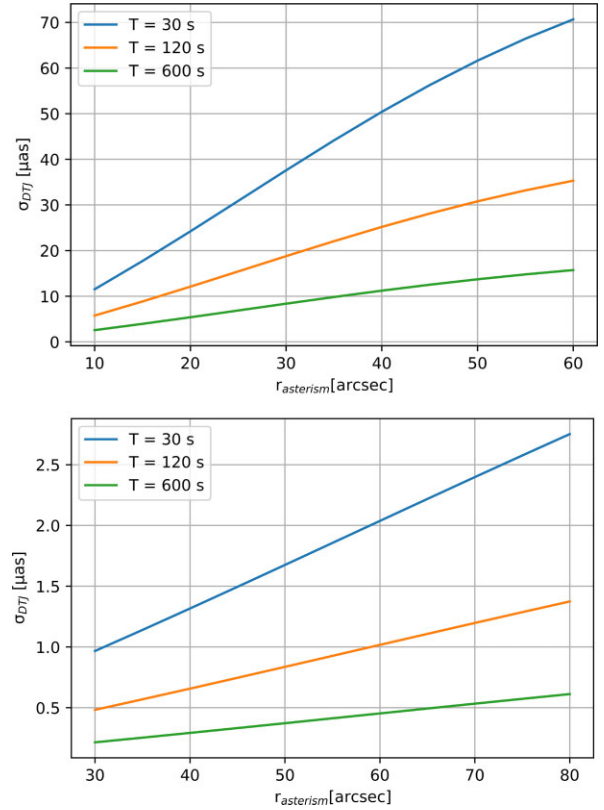


Figure 10. Differential tilt jitter error for targets separation of 1 arcsec as a function of the NGS asterism radius for MAVIS- (top) and MAORY- (bottom) assisted observations. The results are plotted for $T = 30, 120$, and 600 s and show the scaling with $T^{-1/2}$ that has been demonstrated in Section 3.2.

(Cameron et al. 2009; Fritz et al. 2010). We also expect the error to be reduced if an LGS loop controlling the higher orders than the astigmatism is included. In this context, these results have to be considered as an upper limit. An extended study about the impact of the LGS loop residuals on the tip-tilt modes is intended to be the object of future works.

5 CONCLUSION

We have presented an analytical formalism to derive the temporal PSD of the wavefront residuals of an MCAO correction. The formulation includes tomographic, noise, and temporal errors. The general framework allows to select the telescope diameter, the asterism of either NGSs or LGSs, the DMs configuration, the turbulence profile, and the modes of distortion that are sensed through the GSs and compensated by the DMs. We derived an expression for both a closed loop control with an LSE reconstruction and a pseudo-open loop control with an MMSE reconstruction. We applied the results to an NGS-based MCAO configuration in order to analyse the spatial and temporal behaviour of tip-tilt residuals: we found a quadratic dependence of the on-axis residuals on the angular separation of the asterism, that we demonstrated to be consistent with the control of plate-scale distortions operated by the MCAO correction; we also verified the scaling of the residuals with the square root of the scientific exposure time by means of the temporal transfer function of the scientific camera. We analysed differential residuals as well and we provided an analytical expression for the differential tilt jitter error. We showed that the cross-correlations between the GSs of the

asterism and between the GSs and the targets play a role in reducing this source of error with respect to the SCAO case and that parameters like the outer scale and the radius of the asterism can be crucial to properly decrease the differential tilt jitter in MCAO systems. Though these parameters are not under control, it is worth considering them during the preparation of astrometric observations. We finally used our results to quantify the contribution of the differential tilt jitter error to the future astrometric observations, choosing MAORY and MAVIS as case studies. In the case of equilateral asterism of NGSs and considering the possibility of averaging over several exposures, differential tilt jitter should not be the dominant limiting factor to the astrometric precision of these systems.

ACKNOWLEDGEMENTS

The authors thank Carmelo Arcidiacono for fruitful discussion. This work has been partially funded by ADONI – the ADaptive Optics National laboratory of Italy.

DATA AVAILABILITY

No new data were generated or analysed in support of this research.

REFERENCES

- Agapito G., Arcidiacono C., Esposito S., 2017, Proceedings of the fifth Adaptive Optics for Extremely Large Telescopes (AO4ELT5) conference. p. E1
- Ammons S. M., Bendek E. A., Guyon O., 2011, in Shaklan S., ed., Proc. SPIE Conf. Ser. Vol. 8151, Techniques and Instrumentation for Detection of Exoplanets V. SPIE, Bellingham, p. 81510T
- Arsenault R. et al., 2017, *Messenger*, 168, 8
- Basden A. G., Jenkins D., Morris T. J., Osborn J., Townson M. J., 2019, *MNRAS*, 486, 1774
- Beckers J. M., 1988, Very Large Telescopes and their Instrumentation, Vol. 2. European Southern Observatory, Garching, Germany, p. 693
- Bigelow B. et al., 2020, in Marshall H. K., Spyromilio J., Usuda T., eds, Proc. SPIE Conf. Ser. Vol. 11445, Ground-Based and Airborne Telescopes VIII. p. SPIE, Bellingham, p. 1144508
- Cameron P. B., Britton M. C., Kulkarni S. R., 2009, *AJ*, 137, 83
- Chassat F., Rousset G., Primot J., 1989, in Roddier F. J., ed., Proc. SPIE Conf. Ser. Vol. 1114, Active Telescope Systems. SPIE, Bellingham, p. 14
- Cilieggi P. et al., 2020, in Schreiber L., Schmidt D., Vernet E., eds, Proc. SPIE Conf. Ser. Vol. 11448, Adaptive Optics Systems VII. SPIE, Bellingham, p. 114480Y
- Clénet Y., Gendron E., Gratadour D., Rousset G., Vidal F., 2015, *A&A*, 583, A102
- Conan J. M., Rousset G., Madec P. Y., 1995, *J. Opt. Soc. Am. A*, 12, 1559
- Correia C. M., Bond C. Z., Sauvage J.-F., Fusco T., Conan R., Wizinowich P. L., 2017, *J. Opt. Soc. Am. A*, 34, 1877
- Crane J. et al., 2018, in Close L. M., Schreiber L., Schmidt D., eds, Proc. SPIE Conf. Ser. Vol. 10703, Adaptive Optics Systems VI. SPIE, Bellingham, p. 107033V
- Ellerbroek B., 2007, Astrometric Accuracy Limits Due to Tilt Anisoplanatism. TMT Report TMT.AOS.TEC.07.038.REL01
- Ellerbroek B. L., Vogel C. R., 2003, in Tyson R. K., Lloyd-Hart M., eds, Proc. SPIE Conf. Ser. Vol. 5169, Astronomical Adaptive Optics Systems and Applications. SPIE, Bellingham, p. 206
- Flicker R., Rigaut F., 2002, in Vernet E., Ragazzoni R., Esposito S., Hubin N., eds, European Southern Observatory Conference and Workshop Proceedings, Beyond Conventional Adaptive Optics, European Southern Observatory, Garching, Germany, p. 377
- Flicker R., Rigaut F., Ellerbroek B., 2003, *A&A*, 400, 1199
- Fried D. L., 1982, *J. Opt. Soc. Am.*, 72, 52
- Fritz T. et al., 2010, *MNRAS*, 401, 1177
- Fusco T., Conan J.-M., Rousset G., Mugnier L. M., Michau V., 2001a, *J. Opt. Soc. Am. A*, 18, 2527
- Fusco T., Conan J.-M., Michau V., Rousset G., Assemat F., 2001b, in Goglewski J. D., Kamerman G. W., Kohnle A., Schreiber U., Werner C. H., eds, Proc. SPIE Conf. Ser. Vol. 4167, Atmospheric Propagation, Adaptive Systems, and Laser Radar Technology for Remote Sensing. SPIE, Bellingham, p. 168
- Gilles L., Ellerbroek B. L., 2008, *J. Opt. Soc. Am. A*, 25, 2427
- Hardy J. W., 1998, Adaptive Optics for Astronomical Telescopes. Oxford Univ. Press, Oxford
- Le Roux B., Conan J.-M., Kulcsár C., Raynaud H.-F., Mugnier L. M., Fusco T., 2004, *J. Opt. Soc. Am. A*, 21, 1261
- Lindgren L., 1978, in IAU Colloq. 48: Modern Astrometry. p. 197
- Madec P. Y., 1999, in Roddier F., ed., Adaptive Optics in Astronomy. Cambridge Univ. Press, Cambridge, p. 131
- Monty S. et al., 2021, *MNRAS*, 507, 2192
- Negro J. E., 1984, *Appl. Opt.*, 23, 1921
- Neichel B., Fusco T., Conan J.-M., 2008, *J. Opt. Soc. Am. A*, 26, 219
- Noll R. J., 1976, *J. Opt. Soc. Am.*, 66, 207
- Plantet C., Carlà G., Agapito G., Busoni L., 2022, *J. Opt. Soc. Am. A*, 39, 17
- Quiros-Pacheco F., Petit C., Conan J.-M., Fusco T., Marchetti E., 2004, in Bonaccini Calia D., Ellerbroek B. L., Ragazzoni R., eds, Proc. SPIE Conf. Ser. Vol. 5490, Advancements in Adaptive Optics. SPIE, Bellingham, p. 1460
- Rigaut F., Neichel B., 2018, *ARA&A*, 56, 277
- Rigaut F. et al., 2020, in Evans C. J., Bryant J. J., Motohara K., eds, Proc. SPIE Conf. Ser. Vol. 11447, Ground-Based and Airborne Instrumentation for Astronomy VIII. SPIE, Bellingham, p. 114471R
- Rodeghiero G. et al., 2019, preprint ([arXiv:1902.00933](https://arxiv.org/abs/1902.00933))
- Sanders G. H., 2013, *J. Astrophys. Astron.*, 34, 81
- Sandler D. G., Stahl S., Angel J. R. P., Lloyd-Hart M., McCarthy D., 1994, *J. Opt. Soc. America A*, 11, 925
- Sarazin M., Le Louarn M., Ascenso J., Lombardi G., Navarrete J., 2013, in Esposito S., Fini L., eds, Proceedings of the Third AO4ELT Conference. p. 89
- Sasiela R. J., 1994, Electromagnetic Wave Propagation in Turbulence. Evaluation and Application of Mellin Transforms. Springer, Berlin
- Schöck M. et al., 2014, in Marchetti E., Close L. M., Vran J.-P., eds, Proc. SPIE Conf. Ser. Vol. 9148, Adaptive Optics Systems IV. SPIE, Bellingham, p. 91482L
- Tamai R., Koehler B., Cirsuolo M., Biancat-Marchet F., Tuti M., González-Herrera J.-C., 2020, in Marshall H. K., Spyromilio J., Usuda T., eds, Proc. SPIE Conf. Ser. Vol. 11445, Ground-Based and Airborne Telescopes VIII. SPIE, Bellingham, p. 114451E
- Trippie S., Davies R., Eisenhauer F., Förster Schreiber N. M., Fritz T. K., Genzel R., 2010, *MNRAS*, 402, 1126

APPENDIX A: COMPUTATION OF RESIDUAL DISTORTIONS ON A PUPIL PLANE

We use the same notation as Flicker & Rigaut (2002) to relate tip-tilt on the telescope pupil plane with the distortions on a layer of turbulence at altitude h_l . The phase observed at the pupil plane can be seen as a linear combination of tip and tilt:

$$\varphi(\mathbf{x}, \boldsymbol{\theta}, t) = \sum_{k=2}^3 \gamma_k(\boldsymbol{\theta}, t) Z_k(\mathbf{x}/R), \quad (\text{A1})$$

where φ is the phase observed at coordinates \mathbf{x} on the pupil plane for a source at position $\boldsymbol{\theta}$, R is the telescope pupil radius, Z_k is the k th Zernike mode and $\gamma_k(\boldsymbol{\theta}, t)$ are time and field dependent coefficients relating tip-tilt on the pupil plane with all the modes of distortion on a meta-pupil in altitude:

$$\gamma_k(\boldsymbol{\theta}, t) = \sum_{i=2}^N c_{ik}(\boldsymbol{\theta}) A_i(t), \quad (\text{A2})$$

where the coefficients $c_{ik}(\boldsymbol{\theta})$ are defined as (e.g. Negro 1984)

$$\begin{aligned} \mathbf{c}_2(\boldsymbol{\theta}) &= [1, 0, 2\sqrt{3}\theta_x, \sqrt{6}\theta_y, \sqrt{6}\theta_x, 6\sqrt{2}\theta_x\theta_y, \\ &\quad 3\sqrt{2}(3\theta_x^2 + \theta_y^2), 6\sqrt{2}\theta_x\theta_y, 3\sqrt{2}(\theta_x^2 - \theta_y^2), \dots] \\ \mathbf{c}_3(\boldsymbol{\theta}) &= [0, 1, 2\sqrt{3}\theta_y, \sqrt{6}\theta_x, -\sqrt{6}\theta_y, 3\sqrt{2}(\theta_x^2 + 3\theta_y^2), \\ &\quad 6\sqrt{2}\theta_x\theta_y, 3\sqrt{2}(\theta_x^2 - \theta_y^2), -6\sqrt{2}\theta_x\theta_y, \dots] \end{aligned} \quad (\text{A3})$$

and A_i as

$$A_{[2,3]l}(t) = a_{[2,3]l}R/R_l; \quad A_{[4,10]l}(t) = a_{[4,10]l}h_l R/R_l^2; \quad \dots \quad (\text{A4})$$

Due to the orthogonality of the Zernike, the phase variance can be computed as

$$\begin{aligned} \sigma_\varphi^2 &= \text{tr}(C_\gamma) = \sum_{k=2}^3 C_\gamma^{kk} \\ &= \sum_{k=2}^3 \left\langle \left(\sum_{i=2}^N c_{ik}(\boldsymbol{\theta}) A_i(t) \right) \left(\sum_{i=2}^N c_{ik}(\boldsymbol{\theta}) A_i(t) \right)^\dagger \right\rangle, \end{aligned} \quad (\text{A5})$$

where the notation C_γ denotes the covariance matrix of the coefficients $\gamma_k(\boldsymbol{\theta}, t)$.

The SCAO systems compensate for the zeroth order of the distortions, thus the contribution of modes higher than the tilt has to be considered. By exploiting the covariance properties of the Zernike and through straightforward algebra, it can be demonstrated that the

phase variance becomes

$$\begin{aligned} \sigma_\varphi^2 &= \sum_{k=2}^3 \left\langle \left(\sum_{i=4}^N c_{ik}(\boldsymbol{\theta}) A_i(t) \right) \left(\sum_{i=4}^N c_{ik}(\boldsymbol{\theta}) A_i(t) \right)^\dagger \right\rangle \\ &= [(2\sqrt{3}\theta_x)^2 + (2\sqrt{3}\theta_y)^2] \langle A_4(t) A_4^\dagger(t) \rangle \\ &\quad + [(\sqrt{6}\theta_y)^2 + (\sqrt{6}\theta_x)^2] \langle A_5(t) A_5^\dagger(t) \rangle \\ &\quad + [(\sqrt{6}\theta_x)^2 + (-\sqrt{6}\theta_y)^2] \langle A_6(t) A_6^\dagger(t) \rangle + \dots \\ &= 6 \langle A_4(t) A_4^\dagger(t) \rangle + \langle A_5(t) A_5^\dagger(t) \rangle \\ &\quad + \langle A_6(t) A_6^\dagger(t) \rangle (\theta_x^2 + \theta_y^2) + \dots, \end{aligned} \quad (\text{A6})$$

where we showed the results from the first-order distortions. In this case the variance shows to be, at the first order, proportional to the second power of the off-axis separation (i.e. the rms has a linear dependence).

The NGS-based MCAO configuration that we considered is able to compensate for the first-order distortions. The contribution of the uncorrected modes, in this case the ones higher than the astigmatism, leads to a phase variance that is, at the first order, proportional to the fourth power of the off-axis separation (i.e. rms proportional to the second power):

$$\begin{aligned} \sigma_\varphi^2 &= \sum_{k=2}^3 \left\langle \left(\sum_{i=7}^N c_{ik}(\boldsymbol{\theta}) A_i(t) \right) \left(\sum_{i=7}^N c_{ik}(\boldsymbol{\theta}) A_i(t) \right)^\dagger \right\rangle \\ &= 18 \langle A_8(t) A_8^\dagger(t) \rangle + \langle A_9(t) A_9^\dagger(t) \rangle \\ &\quad + \langle A_{10}(t) A_{10}^\dagger(t) \rangle (\theta_x^2 + \theta_y^2)^2 + \dots. \end{aligned} \quad (\text{A7})$$

This paper has been typeset from a \LaTeX file prepared by the author.